# A conservation law model for bidensity suspensions on an incline

Jeffrey T. Wong, Andrea L. Bertozzi

*Department of Mathematics, University of California, Los Angeles,*
*520 Portola Plaza, Box 951555, Los Angeles, CA 90095-1555, USA*

**Abstract**

We study bidensity suspensions of a viscous fluid on an incline. The particles migrate within the fluid due to a combination of gravity-induced settling and shear induced migration. We propose an extension a recent model [N. Murisic, B. Pausader, D. Peschka, and A. L. Bertozzi, *Dynamics of particle settling and resuspension in viscous liquid films*, Journal of Fluid Mechanics **717** (2013), 203–231] for monodisperse suspensions to two species of particles, resulting in a hyperbolic system of three conservation laws for the height and particle concentrations. We analyze the Riemann problem and show that the system exhibits three-shock solutions representing distinct fronts of particles and liquid traveling at different speeds as well as singular shock solutions for sufficiently large concentrations, for which the mechanism is essentially the same as the single-species case. We also consider initial conditions describing a fixed volume of fluid, where solutions are rarefaction-shock pairs, and present a comparison to recent experimental results. The long-time behavior of solutions is identified for settled mono- and bidisperse suspensions and some leading-order asymptotics are derived in the single-species case for moderate concentrations.

*Keywords:* Riemann Problem, bidensity slurry, conservation law

## 1. Introduction

Non-colloidal suspensions of particles in a shear flow exhibit complex interactions within the mixture. These suspensions have many applications, for example in modeling spiral separators used in the mining industry [4]. For suspensions on an incline, the balance of the competing effects of settling due to gravity and shear-induced migration leads to an interesting phenomenon [16, 1]: for low concentrations, there is a 'settled' regime in which the particles and fluid separate into distinct fronts, while for sufficiently high concentrations there is a 'ridged' regime in which only a single particle-rich front appears. Murisic et. al. [11, 12] developed a model for monodisperse suspensions on an incline based on the diffusive flux model of Acrivos [8, 15], which was successfully used to predict the experimentally observed settled and ridged regimes and the time evolution of the fronts. In this model the particles are assumed to be in equilibrium in the normal direction and the leading order system for the film height and particle concentrations form a hyperbolic system of conservation laws with fluxes are determined by a system of ODEs determining the normal equilibrium of the particles. Analysis of hyperbolic systems arising for bidisperse settling have been extensively studied in the context of other models, for instance in the case of settling in a quiescent fluid [2], though not in the incline geometry where we are interested in the long-term dynamics of the fronts rather than the settling of particles to the substrate. The Riemann problem has been studied for the monodisperse model [9, 20], showing the existence of double shock solutions in the settled regime and a transition to singular shocks that occurs in the ridged regime, where particles accumulate at the front. The corresponding rarefaction-singular shock solutions that arise for constant volume initial conditions have also been studied [19].

In this work, we propose an extension of the model to bidisperse suspensions by employing a modification of the diffusive flux model to multiple species [17, 18] and present some preliminary with comparison to recent experiments that build on previous work to identify the qualitative behavior of the fronts in the incline problem [6]. In section 2, we present the model. In section section 3, we describe the Riemann problem for the system and some salient features that are fundamental to understanding the system. Due to the increased complexity of the system, it is more difficult to obtain analytical results, so we describe the system qualitatively and through numerical simulations. We demonstrate that the essential difference from the single species problem is the presence of an additional trailing shock delimiting the transition from heavier to lighter particles, while the remaining two shocks have a similar structure to their monodisperse counterparts. In section section 4, we consider fixed-volume solutions corresponding to results from experiments in which the particles settle to the substrate. We note that the Riemann problem is still relevant here to describe local shock so-

*Email addresses:* jtwong@math.ucla.edu (Jeffrey T. Wong), bertozzi@math.ucla.edu (Andrea L. Bertozzi)

lutions. The full solution has the form of a sequence of rarefaction-shock pairs corresponding to different fronts for the particles and fluid. In section 5 we derive theoretical results for the long-time behavior of monodisperse suspensions in the settled regime, where the concentration of particles uniformly approaches a critical concentration independent of initial conditions. The asymptotic behavior of the front positions is derived, extending the existing results for the high-concentration [19, 20] and dilute limit [12]. The results are then extended qualitatively to the bidisperse problem.

## 2. Model

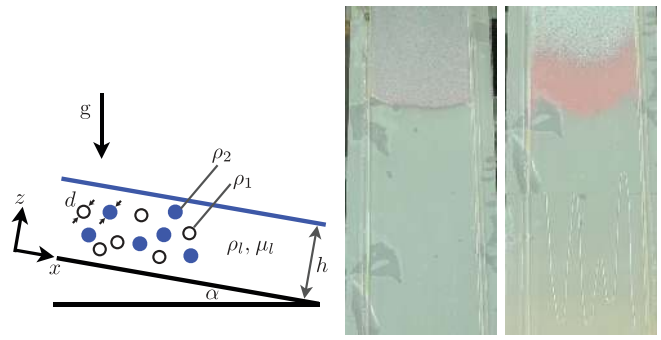


Figure 1: Left; schematic for the incline problem. Center and right; images from a typical experiment [10] with $\alpha = 20\,\text{deg}$, concentrations $\phi_1 = \phi_2 = 0.15$ of each particle type and at times $t = 60\,\text{s}$ and $t = 800\,\text{s}$. The dimensions in the image are $0.14\,\text{m} \times 0.5\,\text{m}$.

Our model is an extension of the dynamic model proposed by Murisic et. al. [12] to multiple species of particles, making use of the equilibrium theory for the diffusive flux model for bidisperse suspensions [18, 5]. Consider a mixture of a fluid with large viscosity $\mu_\ell$ and density $\rho_\ell$ and two species of negatively buoyant particles with diameter $d$ and densities $\rho_{p,1}, \rho_{p,2}$ satisfying $\rho_\ell < \rho_{p,1} < \rho_{p,2}$. The geometry of the system is summarized in Figure 1. The mixture is assumed to be Newtonian with an effective viscosity $\mu(\phi)$ that depends on the particle concentration $\phi$ and density $\rho(\phi) = (1-\phi)\rho_\ell + \phi_1\rho_{p,1} + \phi_2\rho_{p,2}$. The equations for momentum and mass conservation are

$$\rho\frac{\partial \boldsymbol{u}}{\partial t} + \rho\boldsymbol{u}\cdot\nabla\boldsymbol{u} = \boldsymbol{\nabla}\cdot\left(-pI + \mu(\boldsymbol{\nabla u} + \boldsymbol{\nabla u}^T)\right) + \rho\mathbf{g}, \quad (1)$$

$$0 = \frac{\partial \rho}{\partial t} + \nabla\cdot(\rho\boldsymbol{u}) = 0, \quad (2)$$

$$0 = \frac{\partial \phi_i}{\partial t} + \boldsymbol{u}\cdot\boldsymbol{\nabla}\phi_i + \boldsymbol{\nabla}\cdot\boldsymbol{J}_i, \qquad i = 1,2. \quad (3)$$

The expression for viscosity used here is the Krieger-Dougherty relation $\mu(\phi) = \mu_\ell(1-\phi/\phi_{\max})^{-2}$. We note that the order of the zero of $\mu^{-1}$ at $\phi = \phi_m$, which depends on the exponent in the relation, has some effect of the asymptotics for the system that will be discussed in section 4. The flux includes terms due to polydisperse settling [17] and shear-induced diffusion, following the diffusive flux model of Acrivos [7, 15]. This flux is

$$\boldsymbol{J}_{shear} = -\frac{d^2K_c\phi}{4}\nabla(\dot\gamma\phi) - \frac{d^2}{4}\frac{K_v\dot\gamma\phi^2}{\mu(\phi)}\nabla\mu(\phi)$$

where $d$ is the particle diameter, $\dot\gamma$ is the shear rate. and the constants $K_c \approx 0.41$ and $K_v \approx 0.62$ are empirically determined. The flux due to settling for multiple species is

$$\boldsymbol{J}_{settling} = \frac{d^2\mathbf{g}}{18\mu_\ell}\left(M_0(\rho_i - \rho_\ell) + M_I\sum_{j=1}^{2}(\rho_{p,j} - \rho_\ell)\frac{\phi_i}{\phi}\right),$$

where $M_0 = 1 - \frac{\phi}{\phi_m}$ and $M_I = \Phi(\phi)$ are the self- and interaction mobilities [17, 18]. Lastly, we include a flux $J_{tracer}$ (which is small in magnitude) due to shear-induced diffusion [18] that causes mixing between the particle species due to a relative concentration gradient:

$$\boldsymbol{J}_{\text{tracer},i} = -\frac{\dot\gamma d^2}{4}D_{\text{tr}}(\phi)\phi\nabla\left(\frac{\phi_i}{\phi}\right).$$

The derivation of the model equations follows a standard lubrication argument with scales $H/L \ll (d/H)^2 \ll 1$, which asserts that the settling velocity of the particles in the $z$-direction is much greater than that in the $x$-direction. This limits the scope of the model to parameter regimes in which the particles equilibrate quickly in the normal direction and in which the film height is not too small relative to the particle size. As a consequence of the scaling, the leading-order balance in(3) is simply $J_{z,i} = 0$, i.e. the particles are in normal equilibrium. The equilibrium condition then provides a system of ordinary differential equations in $z$ for the particle concentration $\phi$, proportion of lighter particles $X = \phi_1/\phi$ and shear stress $\sigma = \mu(\phi)\frac{\partial u}{\partial z}$ :

$$\sigma' = -1 - \phi\rho(X), \quad (4a)$$

$$X' = c_2\frac{1}{\sigma}\frac{1}{D_{tr}(\phi)}X(1-X)\frac{\phi_{\max}}{\phi_{\max}-\phi}, \quad (4b)$$

$$\phi' = \frac{(\phi_{\max}-\phi)\left(\phi + \rho(X)\left(\phi^2 - B(1-\phi)\right)\right)}{\sigma(\phi_{\max} - (1-c_1)\phi + c_1\phi)}. \quad (4c)$$

Here $\rho(X) = \rho_{s,1}X + \rho_{s,2}(1-X)$ is an average particle density, $B = \frac{2\cot\alpha}{9K_c}$ describes the balance of gravity-induced settling and shear-induced migration and $c_1 = 2(K_v/K_c - 1)$. The velocity profile is obtained from the shear stress as $u(s) = \int_0^{s'}\mu(\phi(s'))^{-1}\sigma(s')ds'$.

To formulate the dynamic equations, define depth averaged concentrations $\phi_i = \int_0^1\tilde\phi_i(s,x,t)ds$ with $\phi = \phi_1 + \phi_2$ and $X = \phi_1/\phi$ using the scaled height $s = z/h(x,t)$. Hereafter, we denote the non-averaged quantities (which depend on $z$ or $s$) with a tilde, e.g. $\tilde\phi(s;x,t)$ is the solution to (4c) subject to a total concentration $\phi(x,t)$ and $X(x,t)$ at position $x$. The fluxes for the system obtained from the

equilibrium solution are then, for $i = 1, 2$,

$$f(\phi, X) = \int_0^1 \tilde{u} ds, \quad g_i(\phi, X) = \int_0^1 \tilde{u}\tilde{\phi}_i ds. \tag{5}$$

The next-order terms in the conservation equations (1) and (3) lead to a system of hyperbolic conservation laws for the film height $h(x,t)$ and integrated particle density $n_i = h\phi_i$:

$$0 = \frac{\partial h}{\partial t} + \frac{\partial}{\partial x}(h^3 f(\phi, X)), \tag{6a}$$

$$0 = \frac{\partial n_i}{\partial t} + \frac{\partial}{\partial x}(h^3 g_i(\phi, X)), \qquad i = 1, 2. \tag{6b}$$

Note that by setting $g = g_1 + g_2$ and $n = n_1 + n_2$ we get a pair of conservation laws for the film height and total number of particles, similar to the monodisperse problem [12]. That system is not closed because $g$ depends on the concentration of both species, so the third equation is necessary. However, the reduced system for $h$ and $n$ informs much of the structure of the full problem, which allows the existing theory to be applied to the bidisperse case.

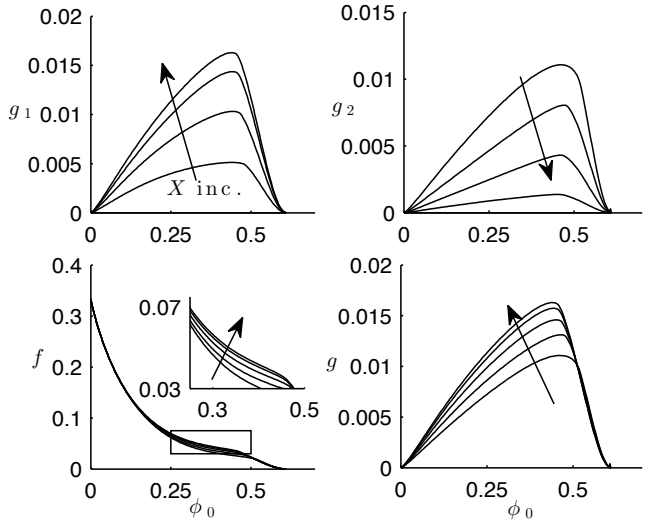


Figure 2: Fluxes for the system (6) as functions of $\phi$ for varying $X$ at $\alpha = 30\,\text{deg}$. Arrows indicate direction of increasing $X$, with $X = 0, 0.25, 0.5, 0.75, 1$. The first row shows the particles fluxes $g_1$ lighter) and $g_2$ (heavier), and the second row shows the fluid flux and the total particle flux $g$.

Before analyzing the Riemann problem we describe a few salient features of the fluxes. In the clear fluid limit, $f = 1/3$ is a constant and $g_i = 0$ in accordance with the Huppert model [3]. For sufficiently large concentrations the fluxes vanish, i.e. there is a maximum packing fraction $\phi_m$ such that $f(\phi_m) = g(\phi_m) = 0$. In addition, for each $X$ there is a unique critical concentration $\phi_c = \phi_c(X) \in (0, \phi_m]$ such that $\phi_c f(\phi_c, X) = g(\phi_c, X)$. This balance will appear frequently in the analysis, so we define

$$R(\phi, X) = \phi f(\phi_X) - g(\phi, X). \tag{7}$$

Physically, the quantity $R$ represents the difference between the difference in effective fluid and particle velocities, so if $R > 0$ then the particles and fluid will tend to separate into distinct fronts and aggregate at a single front if $R < 0$. In the context of the model, we call a state with some concentration $\phi$ and $X$ 'settled' if $\phi < \phi_c$ (i.e. if $R < 0$) and 'ridged' if $\phi > \phi_c$, corresponding to the two regimes observed in experiments.

Plots of the fluxes $f$ (fluid) and $g_i$ (particle $i$), along with $g = g_1 + g_2$, are shown in Figure 2 as functions of $\phi$ and $X$. Hereafter, unless otherwise noted, computed results refer to $\alpha = 30\,\text{deg}$ with parameters corresponding to experiments as in [5]. A few properties of the fluxes are worth noting here. Most importantly, the fluid flux $f$ is insensitive to changes in $X$; it only varies a small amount up to moderate $\phi$ and is nearly constant in $X$ for when $\phi > \phi_{c,2} = \phi_c(0)$ the critical concentration for the heavier particles from the monodisperse theory [11]. Similarly, the total particle flux $g$ is nearly constant in $X$ for $\phi > \phi_{c,2}$ as well, although it varies considerably with $X$ below this threshold (as do the fluxes for each species).

For the fluxes of the equilibrium model, we can look at $\frac{\partial f}{\partial X}$ in more detail to try to understand why it tends to be small, although are more precise estimate is currently lacking. Consider a solution $(\tilde{\phi}, \tilde{X}, \tilde{\sigma})$ to (4) with a given total concentration $\phi$ and $X$. The density difference $\Delta\rho$ is not small, so one might expect there to be a significant dependence on $\rho$. According to the equilibrium theory (as a consequence of (4b), the ODE for $\tilde{X}$), the particle layers are mostly stratified in equilibrium, so we can approximate

$$\tilde{X}(s) = \begin{cases} 0 & s < s_t \\ 1 & s > s_t \end{cases}$$

for some transition point $s_t$ (past which there are no heavier particles). From (4a), the change in shear stress with $X$ is then

$$\frac{d\tilde{\sigma}}{dX}(s) = \begin{cases} (\rho_1 - \rho_2)\phi & s < s_t \\ 0 & s > s_t \end{cases}.$$

The change in $f$ is given by the expression

$$\frac{\partial f}{\partial X} = -\Delta\rho\phi \int_0^{s_t} (1-s)\left(1 - \frac{\tilde{p}hi(s)}{\phi_m}\right)^2 ds - \frac{2}{\phi_m}\int_0^1 (1-s)\left(1 - \frac{\tilde{\phi}}{\phi_m}\right)\sigma\frac{\partial\phi}{\partial X} ds.$$

The first term is due to the change in shear stress and is negative. The second term represents the change in $f$ due to the concentration profile change (which affects the viscosity). The sign of $\frac{\partial\phi}{\partial\tilde{X}}$ is negative for $s < s_t$ (an increase in the number of lighter particles will lead to a smaller total concentration near the substrate). While neither term is particularly small in general, they tend to oppose each other. In the ridged regime, where $\phi$ is increasing, we expect $\frac{\partial f}{\partial\tilde{X}}$ to be small (as is evident in Figure 2) because

$\mu^{-1}$ and $d(\mu^{-1})/d\phi$ will both be small by to the viscosity relation.

## 3. Riemann Problem

We now consider the Riemann problem for the bidisperse system. It is convenient to write the system in vector form, so we define $U = (h, n_1, n_2)^T$ and $F(U) = h^3(f, g_1, g_2)^T$ so that the system is

$$\frac{\partial U}{\partial t} + \frac{\partial}{\partial x} F(U) = 0. \tag{8}$$

The dependence of the flux $F$ on $h$ enters only in the leading factor of $h^3$. If we define a scaled flux $\overline{F} = (f, g_1, g_2)^T$ then the Jacobian of the system is $h^2 \bar{J}$ where $\bar{J}$ depends only on $\phi$ and $X$ and is given by

$$\bar{J} = \left( 3\bar{F} - \phi \frac{\partial \bar{F}}{\partial \phi} \;\middle|\; \frac{\partial \bar{F}}{\partial \phi} + \frac{1-X}{\phi} \frac{\partial \bar{F}}{\partial X} \;\middle|\; \frac{\partial \bar{F}}{\partial \phi} - \frac{X}{\phi} \frac{\partial \bar{F}}{\partial X} \right). \tag{9}$$

Hyperbolicity of the system has been verified numerically over the relevant parameter regime by checking the eigenvalues of (9) over all $(\phi, X)$. We first consider Riemann initial conditions

$$U(x,0) = \begin{cases} U_L & x < 0 \\ U_R & x > 0 \end{cases} \tag{10}$$

(the subscripts indicate the state, e.g. $L$ for left state). Of interest in particular are triple shock solutions, that is, a sequence of shock connections $U_L = U_0 \to U_1 \to U_2 \to U_3 = U_R$ satisfying the Rankine-Hugoniot condition

$$F(U_L) - F(U_R) = s(U_L - U_R) \tag{11}$$

Solutions to (11) for a given left state $U_L$ are a family of three curves ($k$-shocks) corresponding to the eigenvalues $\lambda_1 < \lambda_2 < \lambda_3$ of the Jacobian (9). We impose on each shock $U_{i-1} \to U_i$ with speed $s_i$ the Lax entropy condition

$$\lambda_i(U_{i-1}) > s > \lambda_i(U_i),\ \lambda_{i+1}(U_i) > s > \lambda_{i-1}(U_{i-1}). \tag{12}$$

Shock curves emanating from a state $U$ are denoted here by $S_i^{\pm}(U)$ where $S_i^-$ is the branch satisfying (12). Precise results are somewhat difficult to obtain due not only to the equilibrium ODE, but also to the three-equation system, so we give a qualitative description. As in the monodisperse problem [20], there are three types of triple shock solutions. Typical solutions in each case are shown in Figure 3 in conserved variables $(h, n_1, n_2)$. First, if the concentration of particles is small, the film height is decreasing. For larger concentrations (in the ridged regime), there is a large intermediate height, corresponding to a buildup of particles and fluid near the leading front. For some initial conditions, the two shocks merge together to form a singular shock where the particle concentration reaches the maximum packing fraction. The new feature of the bidisperse system is the presence of the second species, which provides the additional trailing shock. In experiments, we therefore expect to see sharp transitions from a region with heavier particles, to one with lighter particles, and then possibly a clear fluid front depending on the concentration of the mixture, which is what is observed in experiments (for example, in Figure 1).

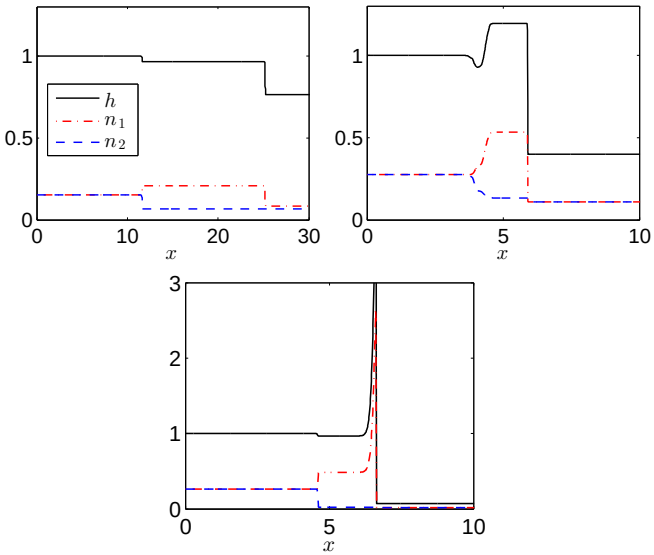


Figure 3: Typical shock solutions for $(h, n_1, n_2)$ with initial states $h_L > h_R$, uniform concentration $\phi_L = \phi_R = \phi_0$ and $X_L = X_R = 0.5$ in the domain. From left to right: a triple shock solution with $\phi_0 = 0.3$ and intermediate state $h^* < h_L$, a solution for large concentration $\phi_0 = 0.55$ with $h^* > h_L$ and a shock/singular shock solution due to a small right state $h_R$.

### 3.1. First shock

We consider now in detail the 1-shock for the bidisperse system, which corresponds to the front of heavier particles. A family of numerically computed shock curves (for different $\phi_L$) are shown in Figure 4. To a good approximation, the curve for small $\phi_L$ represents a jump only in $X$, with $h$ and $\phi$ constant. There is only a small variation in $h$ (representing a small downward jump in film height that can be seen in Figure 3). Note that the admissible states $U_1$ along the shock curve have $X > X_L$, an increase in the concentration of lighter particles. Physically, this represents the lighter particles and fluid separating from the slower front of heavier particles which lags behind while keeping the total concentration across the jump approximately constant. However, as evident in Figure 4, there is some variation in $h$, which is quite prominent as $\phi_L$ becomes large. This is required by the system; it is evident from the expression for the Jacobian (9) that the vector $(0, 1, -1)$ in conserved variables points in the $X$-direction and is a right eigenvector of $J$ only if $\frac{\partial f}{\partial X}$ and $\frac{\partial g}{\partial X}$ are both zero (this is the degenerate case where $h$ and $n$ would form a system independent of $X$). While $\frac{\partial f}{\partial X}$ is small, the same is not true of the latter, so the 1-shock curve cannot only be a jump in $X$ and must have some change in $h$ or $\phi$.

Interestingly, the deviation in the $h$ (and $\phi$) directions increases considerably near and beyond the critical concentration. This can be seen by assuming a formal expansion $h = h_L + h_1 + \cdots$, $\phi = \phi_L + \cdots$ with $h_1 \ll h_L$ where $h_1 \ll h_L$ and the ellipses indicate higher order terms. In this case the $g_1$ equation in (11) gives an estimate for the shock speed:

$$\frac{s}{h_L^2} \approx \frac{1}{\phi_L} \frac{g_1(\phi_L, X) - g_1(\phi_L, X_L)}{X - X_L}. \tag{13}$$

Notably, $g_1$ is approximately quadratic in $X$, which implies that $s$ scales almost linearly with the proportion of lighter particles. Solving for $h_1$ gives the simple approximation

$$\frac{h_1}{h_L} \approx \frac{1}{3} \frac{(\phi f - g)|_{X_L}^{X}}{(\phi f - g)|_{X_L}}.$$

This suggests that $h_1$ depends on the jump in $R = \phi f - g$ from the left to right state. The effect can be seen in Figure 4 (plotting the 1-curve for varying $\phi_L$ and fixed $X_L = 0.5, h_L = 1$). As $\phi_L$ comes close to the ridged regime, the shock curves begin to bend considerably in $h$ due to a large relative change in $R$ (noting that $R(\phi) = 0$ in the transition from settled to ridged).

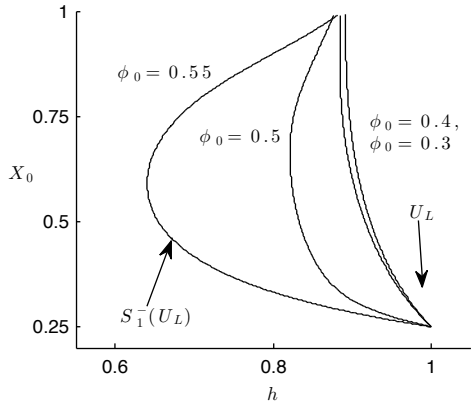


Figure 4: 1-curves for fixed $X_L = 0.25$ and $\phi_L$ varying from 0.3 to 0.55 in the non-conserved variables $(h, \phi, X)$. The curves are nearly parallel to the $X$ axis for $\phi_L$ in the settled regime, representing a transition from mostly heavier to mostly lighter particles with little change in height. For large $\phi_L$, the change in height can be greater if the intermediate state contains a mixture of both particles.

### *3.2. Second and third shocks*

Next, we consider the remaining two shocks. The position of the first intermediate state $U_1$ depends on the right state, which is evident from the family of 2-curves emanating from the 1-curve $S_1^-(U_L)$ (shown in Figure 5). The relevant branch of the curve $S_2^-$ connects states $U_1 \in S_1^- U_L$ to a second intermediate state with a smaller height and total concentration. If $\phi_R$ is small (or $X_R$ is large), i.e. there are few heavy particles downstream, then $X_1$ must

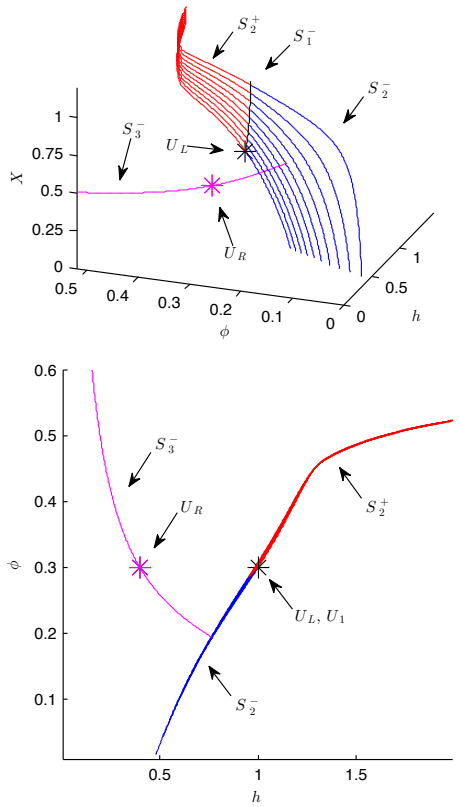


Figure 5: Riemann problem for $\phi$ in the settled regime in the variables $(h, \phi, X)$, in three dimensions (left) and projected onto the $(h, \phi)$ plane (right). The plots show the 1-shock curve (black) from the given left state, family of 2-shock curves emanating from it, and 3-shock curve associated with the given right state.

be near one, so that the last intermediate state $U_2$ has $\phi_2$ sufficiently small (note that $\phi_2 \to 0$ as $X_1 \to 1$).

The family of 2-curves generates a surface in the $(X, \phi)$ plane; a triple-shock solution will exist if the curve of admissible states $U_2$ with $U_2 \to U_R$ intersects this surface. The surface, along with a typical 3-curve is shown in Figure 5. We see that so long as $X_R$ is not too large, the 3-curve will indeed intersect the surface. From the $(h, \phi)$ projection (see right panel in Figure 5, it is clear that we also require $(h_R, \phi_R)$ to be within a certain region, in agreement with the monodisperse theory [9]. If $(h_R, \phi_R)$ lies outside this region, then the 3-connection is instead a rarefaction: $U_0 \to_S U_1 \to_S U_2 \to_R U_R$. Rarefaction solutions are considered in more detail in the context of constant-volume conditions in section 4.

In the case of a ridged left state, the 2-curves satisfying Equation 12 instead have $h$ increasing rather than decreasing; the change in sign of $\phi f - g$ changes which branch of the 2-curve satisfies the entropy condition (this is illustrated in Figure 5, where both $S_2^-$ and $S_2^+$ are shown). The structure of the curves is somewhat more interesting (see [20]) and the asymptotic form is known in the limit as $\phi \to \phi_m$. As $\phi$ increases, the value of $h_L$ increases and diverges to $\infty$, and for sufficiently large $\phi$, the 2 and 3–

curves no longer intersect as $h \to \infty$, which leads to a singular shock. The monodisperse theory applies in this context because the curves in the bidisperse problem collapse almost exactly onto the $(h, \phi)$ plane. Again, as in the settled case, the 2-curves form a surface in the $(\phi, X)$ plane, so that the existence of an intersection $(h^*, \phi^*)$ in the $(h, \phi)$ plane implies there exists some state $U_1$ (by choosing the appropriate $X_1$) such that this is actually an intersection in the full three-dimensional system. Also, we can see that $X \to 1$ as $\phi \to \phi_m$ for the 2 and 3-curves; this implies that only lighter particles aggregate at the singular 'front' (to be expected due to the increased tendency to settle of the heavier particles [5].

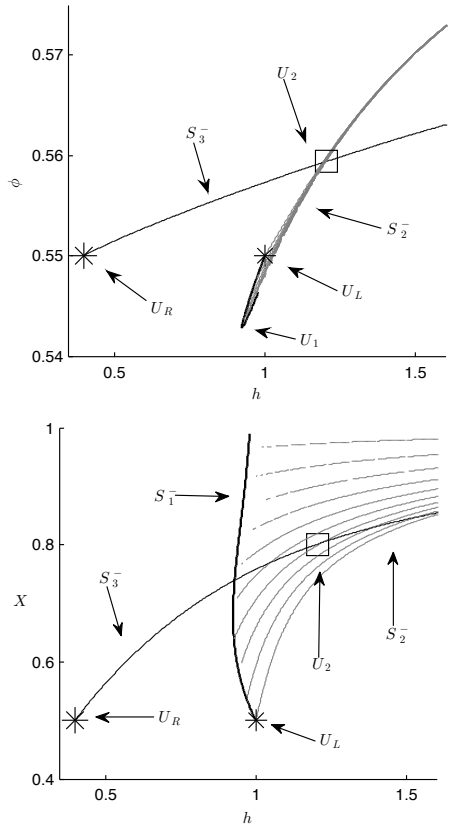


Figure 6: Riemann problem for $\phi$ in the ridged regime projected onto $(h, X)$ and $(h, \phi)$ for left and right states that produce a triple shock with large intermediate height. For smaller choices of $h_R$, the 3−curve (green) will not intersect the family of 2−curves (blue), leading to a singular shock solution, just as in the monodisperse case [20].

## 4. Constant volume solutions

We now look at constant volume solutions to the system (6) in the settled regime. For simplicity, the initial conditions are taken to be $h(x, 0) = 1$ for $x \in [0, 1]$ (zero otherwise) and $n_1(x, 0) = \phi_0 X_0 h(x, 0), n_2(x, 0) = \phi_0(1 - X_0)h(x, 0)$, corresponding to a reservoir of fluid (normalized to length and height one) with some initial

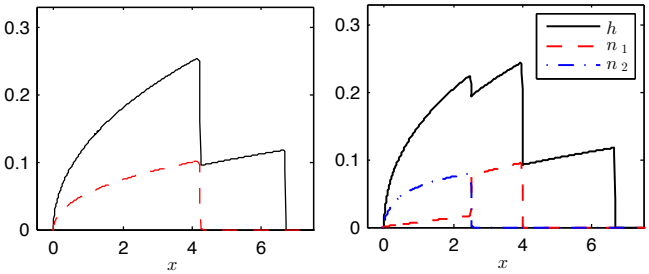


Figure 7: Typical profiles for constant-volume solutions to the mono- and bidisperse system with $\alpha = 30\,\text{deg}$ and $\phi_0 = 0.3$, shown at $t = 500$. The initial conditions are a volume of mixture of height and length one.

volume fraction $\phi_0$. The study of the Riemann problem shows the general structure of solutions as sequences of shocks. The constant-volume solution is instead a series of rarefaction-shock pairs with fronts $x_p(t)$ (the particle front, past which $n = 0$) and $x_f(t)$ (the fluid front). For the bidisperse system, there are two particle fronts $x_{p,2}$ and $x_{p,1}$. Typical solution profiles in both cases are shown in Figure 7.

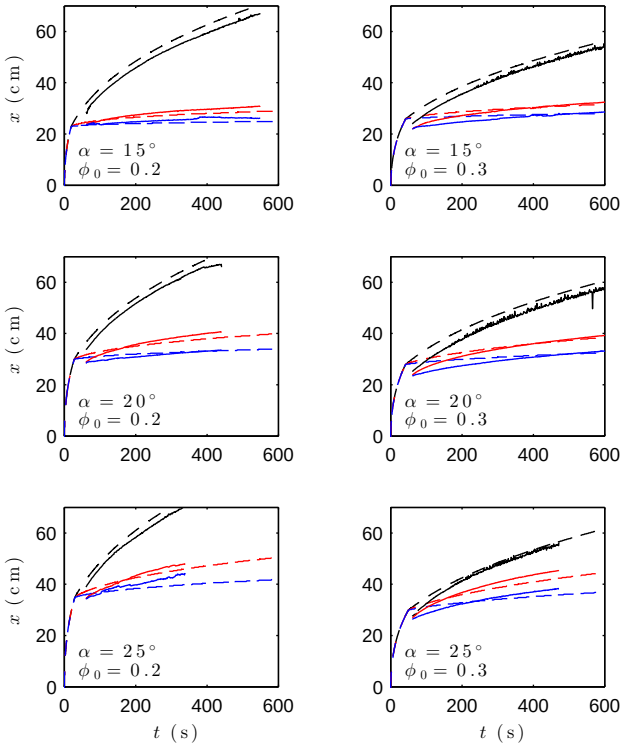


Figure 8: Front positions for the bidisperse system with fixed volume initial conditions for angles $\alpha = 15, 20, 25\,\text{deg}$ (top to bottom) and settled concentrations $\phi_0 = 0.2, 0.3$ (left to right). The solid lines (with dots) are experimental data and dashed lines are numerical solutions.

We can compare, at least qualitatively, the theory pre-

sented here to experimental data. It is challenging to construct the Riemann initial conditions experimentally due to the tendency of particles in the reservoir to settle towards the maximum packing fraction before being released (so that they might not resuspend at all). Experiments testing this model have instead focused on the case of fixed volume initial conditions. Previous investigations have explored the transition between settled and ridged regimes [6]. The experimental data considered [10] has been collected for angles and concentrations within the settled regime (the rarefaction-singular shock pairs expected in the ridged regime [19] have not been fully explored in experiments). The data tracked is the position of the three fronts obtained from imaging, as the height and concentration profiles are difficult to determine accurately. Due to fingering instabilities (visible in Figure 1, particularly for the leading fluid front), the front positions are estimated using an averaging procedure. In addition, because the experiments begin with a well-mixed suspension, some time is required for equilibrium to be reached. This introduces a parameter $t^*$, the time at which the particles reach their equilibrium state. While an estimate can be obtained from a scaling argument, we estimate $t^*$ directly, essentially using it as a fitting parameter. The suspension is evolved as well mixed until $t^*$, (which is within the range of 20 to 40 seconds) and the equilibrium model is used thereafter. A more thorough understanding of the transient phase would be necessary to obtain both a better comparison, and is of interest for future work.

A series of plots comparing the front positions are shown in Figure 8. Solutions to (6) were computed numerically using an upwind scheme, with the fluxes pre-computed from the equilibrium equations(4). As expected, the three fronts can be observed in the experimental data, and the speed of the fronts is greater for larger angles and concentrations. The fluid front is predicted reasonably well. However, the model appears to somewhat under-predict the particle fronts in most cases, particularly for larger angles where the transient phase is expected to be longer. This may be particularly true for multiple species, as the two types of particles must separate from each other as well as from the fluid. While $t^*$ is estimated to be on the order of one minute (so we would hope the model compares well over most of the data), a second transient time might be much later. A suspension that remains partly mixed would behave differently, and for instance might explain the increased speed of the observed front of heavier particles.

## 5. Asymptotic behavior

### *5.1. Long-term behavior: monodisperse*

It is of interest to study similarity solutions that arise as long time limits for these models. The simplest example is the Huppert solution for a clear fluid, which predicts a $t^{1/3}$ scaling for the front position. We can analyze the monodisperse system in detail to obtain the long-term behavior of the fronts and examine the effect of the addition of particles to the $t^{1/3}$ behavior of the Huppert model. The theory for the dilute limit of the dynamic model was studied in [12], where an exact solution for the rarefaction can be found, and the particle front was shown to evolve as $x_p = (C_p t)^{1/3} + T_0 + O(t^{-1/3})$ for some constant $T_0$. A similar behavior occurs in the high-concentration limit, where one obtains a rarefaction and a singular shock [19] and the exponent $\alpha$ in $x_f(t) \sim t^\alpha$ is perturbed slightly from 1/3 due to the accumulation of mass at the front.

We will show that the time scale at which the leading-order asymptotics for the particle fronts become dominant is quite large, and so it cannot be compared directly to the current experimental data. The key observation, used in [19] to approximate the rarefaction in the ridged regime, is that the concentration within the first rarefaction approaches the critical concentration $\phi_c$ as $t \to \infty$. If we define $\phi(\xi) = n(\xi)/h(\xi)$, then it can be shown [19] that necessarily $\phi(0) = \lim_{\xi\to 0} n(\xi)/h(\xi) = \phi_c$ if $n(0) = h(0) = 0$. Since $x_p(t)/t \to 0$ as $t \to \infty$, it must be that $\phi \to \phi_c$ uniformly for $x \in [0, x_p(t)]$ as $t \to \infty$. This suggests that we should look for a solution to (6) with constant concentration, and then study the linearization of $\phi$ about $\phi_c$ to obtain the next-order correction.

To define this solution, let $\xi = x/t$ and let $\lambda(\phi)$ be the largest eigenvalue for (6) (note that $\lambda$ depends only on $\phi = n/h$). The system only admits a rarefaction $n(\xi), h(\xi)$ with $n/h$ constant if $\phi = \phi_c$, so the limiting value of $\phi$ is independent of initial conditions - it is only a function of the system parameters. This solution is, explicitly (as noted in [19] for ridged solutions),

$$h(x,t) = \begin{cases} 0 & \xi < 0 \\ \sqrt{\xi/\lambda_c} & 0 < \xi < x_p(t)/t \\ \sqrt{\xi} & x_p/t < \xi < x_f/t \\ 0 & \xi > x_f/t \end{cases} \tag{14}$$

where the eigenvalue is $\lambda_c = 3f(\phi_c)$. Setting $r := \phi_0/\phi_c$, the front positions are $x_p = (C_p t)^{1/3}$ and $x_f = (C_f t)^{1/3}$ with constants

$$C_p = \frac{9}{4}(3r^2 f(\phi_c)), \qquad C_f = \frac{9}{4}\left(1 - r\left(1 - \sqrt{3f(\phi_c)}\right)\right)^2$$

which can be obtained from particle and fluid conservation

$$\phi_0 = t\int_0^{x_p(t)/t} n(\xi)\,\mathrm{d}\xi \tag{15}$$

$$1 = t\int_0^{x_p(t)/t} h(\xi)\,\mathrm{d}\xi + t\int_{x_p(t)/t}^{x_f(t)/t} \sqrt{\xi}\,\mathrm{d}\xi. \tag{16}$$

Plots of the limiting solution against numerical simulations are shown in Figure 10. For physical context, in the model of [12] with typical experimental parameters, 1500 units of non-dimensional time corresponds to about 10 minutes, by which point the particle fronts have traveled on the order

of one meter along the incline. If the long-time behavior with $\phi \to \phi_c$ is correct, then we expect

$$\lim_{t\to\infty} \frac{x_p(t)}{x_f(t)} = (3r^2 f(\phi_c))^{\frac{1}{3}} \left(1 - r(1 - \sqrt{3f(\phi_c)})\right)^{\frac{2}{3}}. \quad (17)$$

In the dilute limit, the ratio (17) reduces to the result derived by Murisic et. al. [12] with $\phi_c = B/2$.

The behavior of the rarefaction near $\phi_c$ can then be obtained by solving for the concentration $\phi$ in the first rarefaction. Following [19], the ODE system for the rarefaction is (with $\lambda' = \frac{d\lambda}{d\phi}$)

$$h'(\xi) = \frac{1}{h}\frac{1}{2\lambda + \frac{\lambda'}{f'}(\lambda - 3f)},$$
$$n'(\xi) = \frac{1}{h}\frac{\lambda - 3f + \phi f'}{2\lambda f' + \lambda'(\lambda - 3f)}.$$

It follows from the above and the condition $\xi = h^2\lambda$ that

$$\phi' = \frac{1}{\xi}\frac{\lambda(\lambda - 3f)}{2\lambda f' + \lambda'(\lambda - 3f)}. \quad (18)$$

This is a single ODE for $\phi$; the appropriate boundary conditions are $\phi(0) = \phi_c$ as discussed earlier and $\phi(1) = \phi_0$. The entropy condition ensures that the denominator of (18) is single-signed; we can check by computing the eigenvalue explicitly that $\lambda - 3f < 0$ for $\phi < \phi_c$ and $\lambda - 3f > 0$ for $\phi > \phi_c$, so it follows that $\phi_c$ is the unique attracting fixed point as $\xi \to 0$ as expected. We can now linearize (18) about $\phi_c$ and obtain $h = \sqrt{\xi/\lambda(\phi)}$ and $n = h\phi$ from that computation.

There are two cases to consider here, since the fixed point $\phi_c$ may equal $\phi_{\max}$. The linearization depends on the behavior of $R(\phi)$ as defined in (7), which satisfies $R(\phi_c) = 0$. If $\phi_c < \phi_m$ we assume in addition that $R'(\phi_c) < 0$ with the inequality being strict; which should hold for any reasonable model of the fluxes. However, $R'(\phi_m) = 0$, a consequence of the viscosity $\mu(\phi)$ becoming infinite as $\phi \to \phi_m$; more precisely, $R^{(p)}(\phi_m) = 0$ if $\frac{d^p}{d\phi^p}(\mu^{-1})$ as $\phi \to \phi_m$, which holds up to $p = 2$ in the equilibrium model used here [20]. Thus there are two cases to consider for the linearization, depending on whether the degeneracy is present.

Note that for the incline problem, the critical concentration increases with angle, so we can define $\alpha^*$ to be the angle for which $\phi_c = \phi_m$ (if it exists). In the equilibrium model we can find this exactly:

$$\cot\alpha^* = \frac{9\phi_m K_c}{2\rho_s(1 - \phi_m)}(1 + \rho_s\phi_m).$$

For typical experimental parameters, $\alpha^* \approx 15.4\,\text{deg}$, which is well within the range of angles for which the model assumptions are expected to be valid.

*Case 1 ($\phi_c < \phi_m$):*

The scaled eigenvalue $\lambda$ is, explicitly,

$$\lambda = 3f - \frac{R' + 2f}{2} + \frac{1}{2}\sqrt{(R' + 2f)^2 - 12f'R}. \quad (19)$$

Note that this implies (as claimed earlier) that $\lambda \le 3f$ for settled solutions and $\lambda \ge 3f$ for ridged. With $p = \phi - \phi_c$,

$$\lambda - 3f = -3f'(\phi_c)\frac{R'(\phi_c)}{R'(\phi_c) + 2f(\phi_c)}p + O(p^2).$$

The linearization of (18) about $\phi_c$ is therefore

$$p' = \eta\frac{p}{\xi} + O(p^2), \qquad \eta := -\frac{3}{2}\frac{R'(\phi_c)}{R'(\phi_c) + 2f(\phi_c)} \quad (20)$$

so $p \sim K_p\xi^\eta$ to leading order for some constant $K_p$. The prefactor $K_p$ is determined by the constraint $\phi(1) = \phi_0$, but is difficult to obtain explicitly since the approximation is only valid as $\xi \to 0$. We do have, however, the simple approximation $K_p \approx \phi_0 - \phi_c$.

In the equilibrium model it is straightforward to compute the exponent $\eta$ by exploiting the fact that $\phi$ is constant in $z$ at the critical concentration; the result is

$$\eta = -\frac{\beta}{2(\beta + 2)}, \qquad \beta := \frac{1 + 2\rho_s\phi_c + B\rho}{(1 + c_1\frac{\phi_m}{\phi_m - \phi_c})(1 + \rho_s\phi_c)}. \quad (21)$$

Note that $\eta \to 0$ as $\alpha \to \alpha^*$ from above since $\phi_c \to \phi_m$, so the particle concentration will tend to converge more slowly as $\phi_c$ increases.

*Case 2 ($\phi_c = \phi_m$):*

Assume that $R'(\phi_m) = R''(\phi_m) = 0$. and set $p = \phi - \phi_m$. Further assume the expansions

$$R(\phi) = \frac{a}{6}p^3 + O(p^4), \qquad f'(\phi) = bp + O(p^2)$$

Expanding the expression (19) for $\lambda$ gives

$$\lambda = 3f - \frac{R' + 2f}{2} + \frac{1}{2}\sqrt{(R' + 2f)^2 - 12f'R}$$
$$= \left(\frac{3b}{2} - a/2\right)p^2 + O(p^3).$$

The ODE for $\phi$, linearized now about $\phi_m$, is similar to Case 1 with a different exponent:

$$p' = \eta\frac{p}{\xi}, \qquad \eta = -\frac{a}{4b - 2a}. \quad (22)$$

so $p \sim K_p\xi^\eta$. In the equilibrium model, values for $a$ and $b$ have been derived explicitly [20], which allows the exponent to be written in a form analogous to Case 1. The result is

$$\eta = -\frac{\beta}{2(\beta + 2)}, \quad \beta := \frac{\phi_m(1 + \rho_s\phi_m) + B(\phi_m - 1)}{c_1\phi_m(1 + \rho_s\phi_m)}$$

which arise from linearizing (4) about $\phi_m$. The exponent $\eta$ for both cases is plotted in Figure 9; note that there is indeed an angle $\alpha^* \approx 15.4\,\text{deg}$ such that $\phi_c = \phi_m$ for $\alpha < \alpha^*$ according to the model.

We note that $\beta > -1$ is required to ensure that $0 < \eta < 1/2$. But $\beta \to -\infty$ as $\alpha \to 0$, so there is an $\alpha_0$ such that the

above estimate is not valid for $\alpha < \alpha_0$ where $\alpha_0 \approx 7\,\text{deg}$ is quite small. Due to the dominance of settling at small angles and the slow speed of propagation, angles in this small range have not been considered in previous works; it may be of limited interest because the applicability of the model is questionable in this regime.

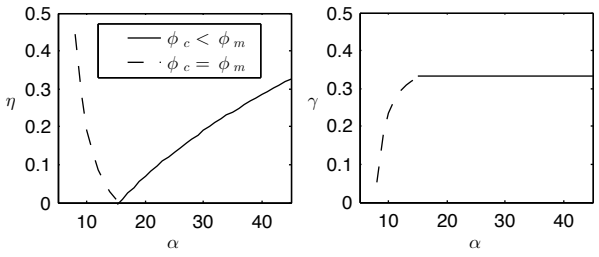


Figure 9: Plot of the exponent $\eta$ in $\phi(\xi) \sim C\xi^\eta$ (left) and growth rate $\gamma$ of the particle front $x_p(t) \sim (C_p t)^\gamma$ against angle $\alpha$ for the equilibrium model when $\phi_c < \phi_m$ (solid, from Eq. (20)) and $\phi_c = \phi_m$ (dashed, from Eq. (22)). The transition occurs at $\alpha^* \approx 15.4\,\text{deg}$; for $\alpha > \alpha^*$, the value of $\gamma$ is 1/3, and for $\alpha < \alpha^*$ it is given by Eq. (23).

*5.2. Front positions: monodisperse*

This can be used to obtain the desired asymptotic behavior for the front positions. Again, we consider the two cases separately.

*Case 1 ($\phi_c < \phi_m$):*

Expanding $h^2\lambda = \xi$ to first-order in $p$ using (20) yields

$$h(\xi) = \frac{\xi^{1/2}}{\sqrt{\lambda(\phi_c)}} - \frac{K_p \lambda'(\phi_c)}{2\lambda(\phi_c)^{3/2}} \xi^{1/2+\eta} + O(p^2).$$

Conservation of particles (15), up to the second term, is then (after some simplification)

$$\phi_0 = t \int_0^{x_p(t)/t} \frac{\phi_c}{\sqrt{\lambda(\phi_c)}} \xi^{1/2} + K_1 \xi^{1/2+\eta}\, \mathrm{d}\xi + \cdots,$$

$$K_1 = \frac{K_p}{\sqrt{\lambda(\phi_c)}} \left( \frac{3f(\phi_c) - g'(\phi_c)}{R'(\phi_c) + 2f(\phi_c)} \right).$$

This yields the leading order term, which is exactly the limiting solution (14), and first correction:

$$x_p(t) \sim (C_p t)^{\frac{1}{3}} + C_{1,p} t^{\frac{1-2\eta}{3}}, \quad C_{1,p} := -K_1 \frac{\sqrt{\lambda_c} C_p^{(1+\eta)/3}}{\phi_c\,(\eta + 3/2)}.$$

The leading order expression for the fluid front can then be determined from fluid conservation (16) to be $x_f(t) \sim (C_f t)^{1/3} + O(t^{(1-2\eta)/3})$, and the ratio of the fronts is then

$$x_p(t)/x_f(t) \sim (C_p/C_f)^{1/3} + O(t^{-2\eta/3}).$$

Note that the factor $\eta$ does not affect the leading order behavior, but controls the time at which the limiting solution becomes the dominant term; the expansion is in powers of $t^{-2\eta/3}$. Since $\eta$ is increasing with $\alpha$ (plotted in Figure 9, left panel), as the inclination angle is decreased, the correction term becomes larger, even approaching $\sim t^{1/3}$ as $\alpha$ approaches the angle for which $\phi_c = \phi_m$. This long time scale for the dominance of the leading order asymptotics is illustrated in Figure 11; the estimate for the front ratios is poor for small angles even up to relatively large times.

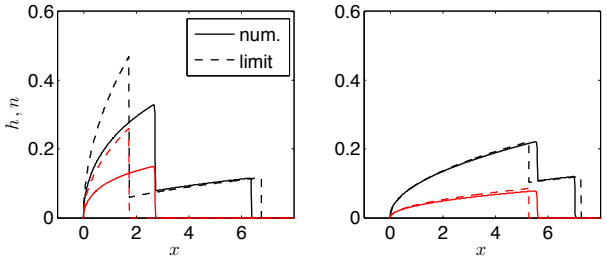


Figure 10: Numerical solution for the monodisperse problem for $\alpha = 20$ (left) and $\alpha = 40\,\text{deg}$ (right) with $\phi_0 = 0.3$ at a moderate time $t = 500$. The dashed lines are the limiting solution (14). The agreement is good for large $\alpha$ but becomes slow to converge as $\alpha$ decreases, in accordance with the asymptotics.

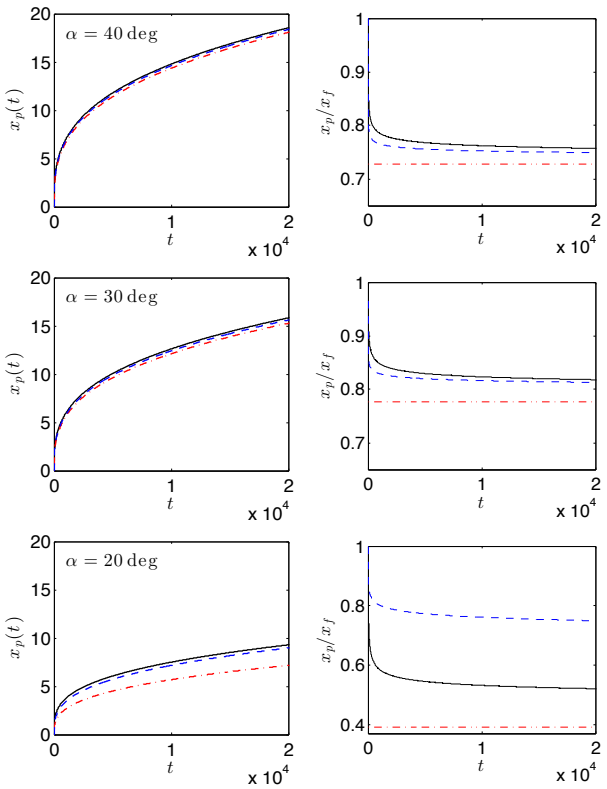


Figure 11: Numerically computed front positions (black) compared to the limiting asymptotics with and without the second term (red and blue, respectively). The left panel shows the particle front, and the right panel shows the ratio of the front positions. The constant $K_p$ is used effectively as a fitting parameter; it is taken to be $K_p = 1$ for $\alpha = 40\,\text{deg}$ and $K_p = 0.66$ for $30\,\text{deg}$ and $K_p = 0.4$ for $20\,\text{deg}$. Note that the agreement is poor for smaller angles, as expected from the asymptotics.

*Case 2 ($\phi_c = \phi_m$):*

Here the linearization of $h$ about $\phi_m$ takes a different form because the denominator of the rarefaction ODE for $h$ vanishes at $\phi = \phi_m$:

$$h = \frac{\sqrt{\xi}}{\sqrt{\lambda}} \sim \frac{1}{|K_p|\sqrt{3b/2 - a/2}} \xi^{1/2-\eta}.$$

Note that unlike the first case, $h$ is not asymptotic to $\sqrt{\xi}$ as $\xi \to 0$. As a consequence, (15) suggests that the particle front to leading order is

$$x_p(t) \sim (C_p' t)^\gamma + \cdots \quad \gamma := \frac{1-2\eta}{3-2\eta} \tag{23}$$

for some constant $C_p'$. In contrast, the rarefaction for the clear fluid is given exactly by $\sqrt{\xi}$, and so volume conservation (16), implies that $x_f(t) \sim (C_f t)^{1/3}$ to leading order for $C_f = \frac{9}{4}(1 - \phi_0/\phi_m)^2$. Thus $x_p$ grows asymptotically slower than $x_f(t)$ (since $\eta > 0$), so $x_p/x_f \to 0$ as $t \to \infty$ in contrast to the $\phi_c < \phi_m$ case or the dilute limit. In the ridged regime, the decrease in the asymptotic front speed to $x_p(t) \sim t^\gamma$ occurs due to mass accumulation at the (singular) shock [19]. Here, the deviation is due to accumulation of particles to the maximum packing fraction in the back of the fluid rather than the front, and the leading clear fluid front is unaffected. This establishes two qualitatively different long-term behaviors - for large angles ($\phi_c < \phi_m$), the ratio $x_p(t)/x_f(t)$ approaches a constant as $t \to \infty$ while for small angles ($\phi_c > \phi_m$) the particle front lags arbitrarily far behind the fluid front as the concentration in the particle-laden region approaches $\phi_m$. However, because the rate of convergence is so slow, it may be difficult to verify this distinction between the two cases in an experiment.

### *5.3. Long-term behavior: bidisperse*

For the bidisperse problem (6), the computations are made much more cumbersome due to the third equation. We can, at least, identify the corresponding limiting solution under the assumption that it exists. Consider initial conditions as in the monodisperse case, but with $n_1(x,0) = \phi_1 h(x,0)$ and $n_2(x,0) = \phi_2 h(x,0)$ (with $\phi_1 = \phi_0 X_0$ and $\phi_2 = \phi_0(1 - X_0)$). The initial conditions are assumed to be settled: $\phi < \phi_{c1}, \phi_{c2}$.

It is easy to show that a constant concentration rarefaction can only exist if $\phi = \phi_c(X)$ and $X = 0$ or $X = 1$, which suggests that the long-time behavior has a rarefaction with only heavier particles ($\phi = \phi_{c,2}$), then a rarefaction with only lighter particles ($\phi = \phi_{c,1}$), and finally a clear-fluid front. Numerical evidence suggests this is the case (see Figure 12), although convergence of the heavier particle layer to $X = 0$ - if at all - is quite slow (even slower, perhaps, than the already slow convergence of $\phi$ to $\phi_c$).

By assumption, there exists a unique $\phi_c(X)$ such that $\phi_c f(\phi_c) = g(\phi_c)$. If $\lambda$ and $r = (r_1, r_2, r_3)^T$ are the eigenvalue/eigenvector for the rarefaction, then $h' = \alpha r_1, n_1' = \alpha r_2$ and $n_2' = \alpha r_3$ where $\alpha = \frac{1}{D\lambda \cdot r}$. If $\phi_1$ and $\phi_2$ are constant then $r_2/r_1 = \phi_1$ and $r_3/r_1 = \phi_2$, so the eigenvector is $r = (1, \phi_1, \phi_2)^T$. Simplifying $Jr = \lambda r$ where $J$ the Jacobian (9) then gives $3(f, g_1, g_2) = \lambda(1, \phi_1, \phi_2)$, so we have $\lambda = 3f$ (as before) along with $g_1 = \phi_1 f$ and $g_2 = \phi_2 f$. Thus $g = \phi f$, which implies that $\phi = \phi_c(X)$ with $X = \phi_1/\phi$. Moreover, it can be checked directly that the individual equalities cannot hold when $\phi = \phi_c(X)$ unless $X = 0$ or $X = 1$ (where it reduces to the monodisperse case).

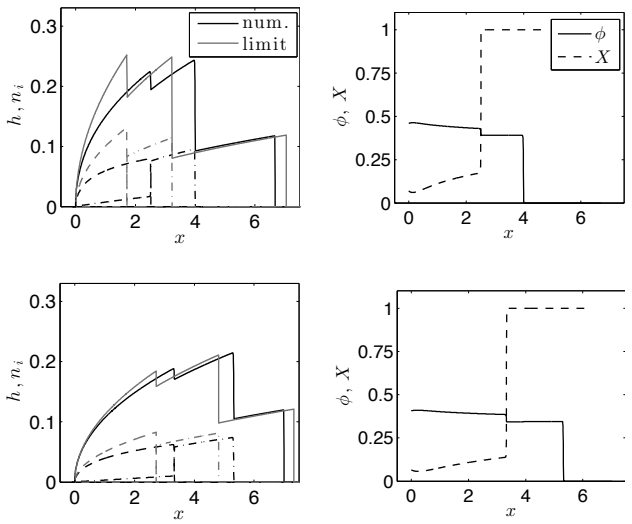


Figure 12: Numerical solution (solid) and limiting solution (24) (dashed) for the bidisperse problem at $t = 500$ with $\phi_0 = 0.3$ and $\alpha = 30\,\text{deg}$ (top) and $\alpha = 40\,\text{deg}$ (bottom). The right panels show $\phi$ and $X$; note that $X \approx 1$ in the second rarefaction. For very long times, $X \to 0$ in the first rarefaction, i.e. the particle species separate.

This suggests that the long-time behavior should consist of a rarefaction with only heavier particles ($\phi = \phi_{c,2}$), then a rarefaction with only lighter particles ($\phi = \phi_{c,1}$), and finally a clear-fluid front. Numerical evidence suggests this is the case (see Figure 12), although convergence of the heavier particle layer to $X = 0$ - if at all - is quite slow (even slower, perhaps, than the already slow convergence of $\phi$ to $\phi_c$). The precise solution is essentially the same as (14) so long as $\phi_{c,i} < \phi_m$ for $i = 1, 2$:

$$h(x,t) = \begin{cases} 0 & \xi < 0 \text{ or } x_f/t < \xi \\ \sqrt{2A_2\xi} & 0 < \xi < x_2(t)/t \\ \sqrt{2A_1\xi} & x_2(t)/t < \xi < x_1(t)/t \\ \sqrt{\xi} & x_1(t)/t < \xi < x_f(t)/t \end{cases} \tag{24}$$

where $2, 1, f$ denote the fronts for the heavier particle, lighter particle and fluid, respectively. The constants are $A_2 = \frac{1}{6f(\phi_{c2},0)}$ and $A_1 = \frac{1}{6f(\phi_{c1},1)}$. The fronts are $x_i(t) = (C_i t)^{1/3}$ for $i = 1, 2$ and $x_f(t) = (C_f t)^{1/3}$ where

$$C_2 = \frac{9\phi_2^2}{8A_2\phi_{c2}^2}, \quad C_1 = \frac{9\phi_1^2}{8A_1\phi_{c1}^2}\left(1 + \frac{\phi_{c1}}{\phi_{c2}}\sqrt{\frac{A_1}{A_2}}\frac{(1-X_0)}{X_0}\right)^2.$$

Finally the constant for the fluid is

$$C_f = \frac{9}{4}\Big(1 - \sum_{i=1}^{2} \frac{\phi_i}{\phi_{c,i}}\left(1 - \sqrt{1/2A_i}\right)\Big)^2.$$

Typical solutions are shown in Figure 12. The convergence is not very fast and we need to have $X \to 0$ (or $X \to 1$) as well as $\phi_i \to \phi_{c,i}$ in the appropriate regions. For $X_0 < 1$, the ratio of the front positions for the particles is

$$\lim_{t\to\infty} \frac{x_{p2}(t)}{x_{p1}(t)} = \left(1 + \frac{X_0}{(1-X_0)}\frac{\phi_{c2}}{\phi_{c1}}\sqrt{\frac{f(\phi_{c1},1)}{f(\phi_{c2},0)}}\right)^{-2/3}.$$

As in the monodisperse case, if $\phi_{c,i} > \phi_m$ then we expect the limiting ratio $x_{p,i}/x_f$ to be zero.

## 6. Discussion

We have presented a conservation law model for bidisperse suspensions on an incline, extending the model of Murisic et. al. [12] to multiple species. The Riemann problem exhibits triple shock solutions that describe the evolution of the particle and fluid fronts. The addition of a second species leads to separation between the two types of particles, producing a trailing shock across which the composition of particles changes from mostly heavier to mostly lighter particles while the total concentration is nearly constant. The structure of the Riemann problem is otherwise similar to the single-species case, including the distinction between settled and ridged regimes and the formation of singular shocks [19, 20]. In the case of multiple species, the first shock (for the heavier particles) is always present while the singular shock can only appear for the front of lighter particles.

We have studied constant-volume solutions in the settled regime, which correspond to experiments where a fixed volume of a mixture is released down the incline. In the model, solutions are three rarefaction-shock pairs with mostly heavier particles, then lighter particles, then clear fluid. Preliminary comparison to experimental data shows reasonable qualitative agreement; the general structure of three shocks separating the two particle species and the fluid front is observed in the settled regime, but the front positions are consistently under-predicted by the model. Because the model relies on the assumption that particles are in equilibrium, it cannot be compared to the experimental data at early to moderate times where the suspension may still be partly mixed. A model appropriate to the transient phase may be necessary to better understand the system at early times, and make comparison easier at later times when the model should be applicable. The discrepancies between the current bidisperse model and experiments seem to suggest that the model could be improved; a long transient time due to mixing between the two species is a significant concern.

An adjustment to the equilibrium model by way of different physics would manifest itself as a change in the fluxes for the dynamic equations, producing a similar qualitative behavior. While simple, the general diffusive flux model from which we obtain the fluxes has been successful in comparing to experiments in the monodisperse case. It is not always an accurate reflection of the physics of the problem, particular at concentrations near the maximum packing fraction where models based on normal stress differences are more appropriate [13, 14]. This is primarily a concern in the ridged regime (which is not the focus here), where the particle concentration approaches $\phi_m$ at the front, and in the derived asymptotics for small angles, where this occurs in the back of the particle rarefaction.

In the constant-volume case, we have derived the asymptotic behavior of the front positions for the monodisperse model in the settled regime and applied this to find the leading order behavior for bidisperse suspensions. The front positions are shown to evolve as $t^{1/3}$ except at small angles, where the concentration approaches the maximum packing fraction in the rarefaction and ratio of particle to fluid fronts tends to zero. The slow rate of convergence, however presents a significant challenge for experimental comparison, as the time scale at which the asymptotic behavior becomes dominant is large (perhaps prohibitively so) except at large angles $\alpha \approx 40\,\text{deg}$). It would be interesting, though, to see if this transition could be observed in experiments.

*Acknowledgements*

We thank Li Wang and Dirk Peschka for helpful conversations, and Sarah Burnett, Andrew Li, Matthew Molinaire and Katherine Varela for their experimental work. This work is funded by NSF grants DMS-1312543 and DMS-1045536.

[1] B. P. Cook, *Theory for particle settling and shear-induced migration in thin-film liquid flow*, Phys. Rev. E. **78** (2008), 045303.

[2] Robert Dorrell and Andrew J Hogg, *Sedimentation of bidisperse suspensions*, International Journal of Multiphase Flow **36** (2010), no. 6, 481–490.

[3] Herbert E Huppert, *Flow and instability of a viscous current down a slope*, Nature **300** (1982), no. 5891, 427–429.

[4] S. Lee, Y. M. Stokes, and A. L. Bertozzi, *Behavior of a particle-laden flow in a spiral channel*, preprint, 2014.

[5] S. Lee, Jeffrey Wong, and A. L. Bertozzi, *Particle-laden flows of bidensity suspensions*, Mathematical Modelling and Numerical Simulation of Oil Pollution Problems, vol. 2, Springer Verlag, 2015.

[6] Sungyon Lee, Aliki Mavromoustaki, Gilberto Urdaneta, Kaiwen Huang, and AndreaL. Bertozzi, *Experimental investigation of bidensity slurries on an incline*, Granular Matter **16** (2014), no. 2, 269–274 (English).

[7] D. Leighton and A. Acrivos, *Shear-induced migration of particles in concentrated suspensions*, Journal of Fluid Mechanics **181** (1987), 415.

[8] David Leighton and Andreas Acrivos, *Measurement of shear-induced self-diffusion in concentrated suspensions of spheres*, Journal of Fluid Mechanics **177** (1987), 109–131.

[9] A Mavromoustaki and AL Bertozzi, *Hyperbolic systems of conservation laws in gravity-driven, particle-laden thin-film flows*, Journal of Engineering Mathematics (2014), 1–20.

[10] Matthew Molinaire, Andrew Li, Sarah Burnett, and Katherine Varela, *Gravity driven particle-laden flow*, `ftp://ftp.math.ucla.edu/pub/camreport/cam15-11.pdf`, 08 2014.

[11] N. Murisic, J. Ho, V. Hu, P. Latterman, T. Koch, K. Lin, M. Mata, and A. L. Bertozzi, *Particle-laden viscous thin-film*

*flows on an incline: experiments compared with an equilibrium theory based on shear-induced migration and particle settling*, Physica D **240** (2011), no. 20, 1661–1673.

[12] N. Murisic, B. Pausader, D. Peschka, and A. L. Bertozzi, *Dynamics of particle settling and resuspension in viscous liquid films*, Journal of Fluid Mechanics **717** (2013), 203–231.

[13] P. R. Nott and J. F. Brady, *Pressure-driven flow of suspensions: simulation and theory*, J. Fluid Mech. **275** (1994), 157–199.

[14] Prabhu R Nott, Elisabeth Guazzelli, and Olivier Pouliquen, *The suspension balance model revisited*, Physics of Fluids (1994-present) **23** (2011), no. 4, 043304.

[15] Ronald J. Phillips, Robert C. Armstrong, Robert A. Brown, Alan L. Graham, and James R. Abbott, *A constitutive equation for concentrated suspensions that accounts for shear-induced particle migration*, Physics of Fluids A: Fluid Dynamics **4** (1992), no. 1, 30–40.

[16] Arun Ramachandran and David T Leighton Jr, *The effect of gravity on the meniscus accumulation phenomenon in a tube*, Journal of Rheology (1978-present) **51** (2007), no. 5, 1073–1098.

[17] J. M. Revay and J. J. L. Higdon, *Numerical simulation of polydisperse sedimentation: equal-sized spheres*, Journal of Fluid Mechanics **243** (1992), 15–32.

[18] Anubhav Tripathi and Andreas Acrivos, *Viscous resuspension in a bidensity suspension*, International Journal of Multiphase Flow **25** (1999), no. 1, 1 – 14.

[19] Li Wang, A Bertozzi, G. Urdaneta, and K. Huang, *Rarefaction-singular shock dynamics for conserved volume gravity driven particle-laden thin film*, Physics of Fluids (2015), To appear.

[20] Li Wang and Andrea L Bertozzi, *Shock solutions for high concentration particle-laden thin films*, SIAM Journal on Applied Mathematics **74** (2014), no. 2, 322–344.